Simultaneous Control of Two Points for Snake Robot and Its Application to Transportation

Mizuki Nakajima[1], Motoyasu Tanaka[1], and Kazuo Tanaka[1]

***Abstract*—The paper presents a simultaneous trajectory tracking control method for two points of a snake robot. The kinematic model considering two regulated points is determined as a switched system that is switched by lifting a few wheels. The system becomes a kinematically redundant system by the lifting of the wheels; however, it has to prevent two types of singular configurations; one is the traditional one, and the other is caused by regulating two points simultaneously. Using this redundancy and selecting the lifted wheels, we design a trajectory tracking controller for two points by preventing the two types of singular configurations. The effectiveness of the proposed control method was demonstrated by tracking experiments as well as applications, namely, the transportation of an object by caging manipulation and the steering of a handcart.**

***Index Terms*—Biologically-Inspired Robots, Redundant Robots, Wheeled Robots.**

I. Introduction

SNAKE robots have long and thin bodies and can locomote on uneven terrain [1], [2], under water [3], [4], and on/in piping [2], [5]–[7]. These features indicate the effectiveness of snake robots for application as inspection robots in narrow spaces where humans cannot enter and as disaster response robots. In these cases, the robot moves to the desired point by remote control or autonomous control. It is highly challenging for humans to directly operate all the joints of a snake robot because of the excessively high number of joints. Therefore, numerous research studies have been conducted on the control of a snake robot, such as [8].

Hirose has proposed a *serpenoid curve* based on the motion of a snake; the locomotion of a snake robot by lateral undulation was accomplished by using the curve [9]. A motion emulating the following locomotions of snakes has been accomplished; sinus-lifting [10], [11], sidewinding [11]–[13], and concertina [14]. Certain researchers have focused on the central pattern generator and have proposed optimization of the undulation [3] and a method for collision prevention [15]. As a serpenoid curve, the control method which regulates the forward speed and orientation of the center of gravity using virtual constraints as [16]. By using kinematic constraints caused by passive wheels, the trajectory tracking methods in which the convergence to arbitrary trajectories is guaranteed have been proposed [17]–[21]. Three-dimensional trajectory tracking by lifting the head has also been proposed [22]–[25].

Researches related to inspection and operation by snake robots have been conducted. The transportation task has been proposed by cooperative control of two snake robots [26]. A control method for underwater inspection work has been proposed by controlling the robot like a manipulator [4]. Tanaka has proposed task-space control method for a snake robot with active wheels equipped with a gripper at the head, and various operations have been accomplished; the picking up an object, rotating valve, and opening small door [27]. In these researches, the robots contacted the object with the robot's head or an effector attached to the head. In contrast, if both the head and tail can be regulated, the robot is likely to be operable as a dual-arm robot by using the head and tail as two arms and capable of transporting an object by using caging [28].

This paper presents a control method that causes both the head and an additional point of a snake robot to converge to each target trajectory. The effectiveness of the proposed control method is demonstrated by an experiment for verifying the trajectory tracking and two others (transporting an object using caging manipulation and pushing a handcart) for verifying its applicability.

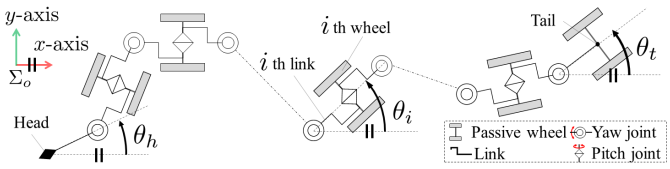

(a) Pattern diagram. Dotted lines are auxiliary line. θ_h and θ_t represent the orientation of the head and the tail, respectively. θ_i represents the orientation of the ith wheel.

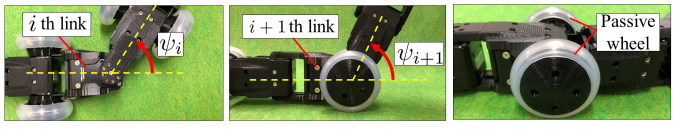

(b) Closed view of the real robot. Yellow dotted lines are auxiliary line. ψ_i represents the ith joint angle.

Fig. 1. A model of a snake robot.

Manuscript received: June 4, 2019; Revised: September 2, 2019; Accepted: October 3, 2019.

This paper was recommended for publication by Editor Yu Sun upon evaluation of the Associate Editor and Reviewers' comments. This work was partially supported by the ImPACT Program of Council for Science, Technology and Innovation (Cabinet Office, Government of Japan) and JSPS KAKENHI Grant Number 18K04011.

[1]The authors are with the Department of Mechanical and Intelligent Systems Engineering, The University of Electro-Communications, Tokyo 182-8585, Japan (email: mizuki.nakajima@rc.mce.uec.ac.jp).

Digital Object Identifier (DOI): see top of this page.

II. Problem Setting

We use the snake robot shown in Figure 1. The robot has $2n$ links, which are serially connected by $2n-1$ active joints. Let l be the length of each link. The yaw and pitch joint are alternately connected as shown in Fig. 1(a). The first joint is a yaw joint. Let ψ_i be the ith joint angle; moreover, we set $\boldsymbol{\psi} = [\psi_1, \psi_2, \cdots, \psi_{2n-1}]^\top \in \mathbb{R}^{2n-1,1}$. The joint angle ψ_i is the angle between the ith link and the $i+1$th link as shown in Fig. 1(b). A pair of passive wheels is mounted coaxially to both the pitch joint and tail, and the total number of pairs of wheels is n. Let θ_h be the orientation of the head, θ_t be the orientation of the tail, θ_i be the orientation the ith wheel. The passive wheel has a large friction in the side direction and negligible friction in the longitudinal direction. The robot locomotes by undulation using anisotropic friction. Silicon tires have been used in the actual robot as shown in Fig. 1(b). The coefficient of static friction of the tire is 0.77. It was measured by preliminary experiment. It is sufficiently large for locomotion of the robot.

We assume that the environment is a flat plane. Let Σ_o be the fundamental coordinate system on the plane. Let the first and second control points be the two points that are being regulated. The control objective of the study is that the two control points track the arbitrary target trajectories. We define that the first control point is the head of the robot and the second control point to be the center of an arbitrary wheel axle.

Here, we consider the case where we permit the second control point to move and fix the first control point. In the case where all the wheels touch the ground, the motion of the second control point is prevented by the friction of the wheels. If the sideslip of the wheel is not permitted, the robot can neither move the second control point nor rotate all the joints. If the sideslip of the wheel is permitted, the robot can rotate all the joints; however, the motion results in error in the position and orientation of the head, as in [32].

Thus, we introduce lifting wheels by using the pitch joint, as in Fig. 2 and [17], [21], [31], [32]. By marginally lifting a few wheels, we can eliminate the velocity constraints corresponding to the wheels that are lifted. As a result, the lifted wheel can move to the side direction. However, even if the number of lifted wheels is adequate, the motion of the second control point is likely to be limited depending on the robot posture. This singular configuration is unique in the tracking control of two points; moreover, it is independent of the traditional singular configuration [29], which occurs when the robot regulates the head. We denote the traditional one as singular configuration I and the one unique to two-point control as singular configuration II. The two types of singular configuration depend on the allocation of grounded/lifted wheels. Therefore, the robot can prevent the two types of singular configuration by changing the allocation of grounded/lifted wheels at regular time intervals. The details of these singular configurations are discussed in Section IV.A based on the control models, the control inputs, and the closed loop of the system.

III. Kinematic Model

The snake robot locomotes by lateral undulation using the anisotropic friction of the wheels that touch the ground. We assume that the wheels that touch the ground do not slide. In addition, the angles of pitch joints for the lifting are very small, and the influence on the two dimensional motion of the robot is small. Therefore, it is approximated to zero in the control model [17], [21], [30]–[32]. Let ϕ_i be the angle of the ith yaw joint; moreover, we set $\boldsymbol{\phi} = [\phi_1, \phi_2, \cdots, \phi_n]^\top \in \mathbb{R}^{n,1}$. Let $\boldsymbol{p}_i = [x_i, y_i, \theta_i]^\top$ be the vector that combines the center position of the ith wheel axle and orientation of the ith wheel, $\boldsymbol{p}_h = [x_h, y_h, \theta_h]^\top$ be the vector that combines the position and orientation of the head. The velocity constraint that implies that the ith wheel does not skid is represented as

$$\dot{x}_i \sin\theta_i - \dot{y}_i \cos\theta_i = 0. \tag{1}$$

By considering (1) for all the wheels, we obtain

$$\boldsymbol{A}\dot{\boldsymbol{p}}_h = \boldsymbol{B}\dot{\boldsymbol{\phi}}, \tag{2}$$

where $\boldsymbol{A} \in \mathbb{R}^{n,3}$ and $\boldsymbol{B} \in \mathbb{R}^{n,n}$.

We introduce switching constraints to (2) as in [17], [21], [31], [32]. The robot changes the allocation of the grounded/lifted wheels every t_σ seconds. This implies that the robot moves by switching the model. We represent the allocation of the grounded/lifted wheels by the unique integer σ and call it *mode*. The mode $\sigma(t)$ is represented as

$$\sigma(t) \quad = \quad \sigma_k, \qquad (t_k \le t < t_{k+1}) \tag{3}$$

where $t_k = kt_\sigma (k = 0, 1, \cdots)$. The total number of values of σ is 2^n. However, it includes the infeasible/inappropriate mode; e.g., the mode wherein all the wheels are lifted is infeasible, and the mode wherein all the wheels touch the ground is inappropriate because the control objectives cannot be obtained. These modes should be excluded from the mode candidates. The details for reducing the mode candidates are described in Section IV.C.

The velocity constraint in mode σ is represented as

$$\boldsymbol{A}_\sigma \dot{\boldsymbol{p}}_h = \boldsymbol{B}_\sigma \dot{\boldsymbol{\phi}}, \tag{4}$$

$$\boldsymbol{A}_\sigma = \boldsymbol{T}_\sigma \boldsymbol{A} \ , \ \boldsymbol{B}_\sigma = \boldsymbol{T}_\sigma \boldsymbol{B}, \tag{5}$$

where $\boldsymbol{T}_\sigma$ is the selection matrix, which selects the velocity constraints corresponding to the grounded wheel by eliminating that corresponding to the lifted wheel. Letting n_σ be the number of grounded wheels. The sizes of the matrices are $\boldsymbol{T}_\sigma \in \mathbb{R}^{n_\sigma,n}$, $\boldsymbol{A}_\sigma \in \mathbb{R}^{n_\sigma,3}$, and $\boldsymbol{B}_\sigma \in \mathbb{R}^{n_\sigma,n}$. The rows corresponding to the grounded wheels are selected from the original matrix by the selection matrix.

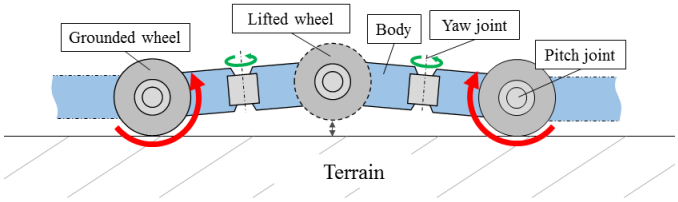

Fig. 2. The wheel is lifted by adjacent pitch joints.

Next, we introduce $\boldsymbol{p}_k = [x_k, y_k, \theta_k]^\top$, which is the position of the kth wheel and the absolute angle of the link that has the kth wheel, to the model as the second regulated point. By differentiating $\boldsymbol{p}_k$, the kinematic relation is obtained as

$$\dot{\boldsymbol{p}}_k = \begin{bmatrix} \boldsymbol{J}_1 & \boldsymbol{J}_2 \end{bmatrix} \begin{bmatrix} \dot{\boldsymbol{p}}_h \\ \dot{\boldsymbol{\phi}} \end{bmatrix}, \tag{6}$$

where $\boldsymbol{J}_1 \in \mathbb{R}^{3,3}$ and $\boldsymbol{J}_2 \in \mathbb{R}^{3,n}$. Considering (4) and (6), we obtain

$$\tilde{\boldsymbol{A}}_\sigma \dot{\tilde{\boldsymbol{w}}} = \tilde{\boldsymbol{B}}_\sigma \dot{\boldsymbol{\phi}}, \tag{7}$$

$$\tilde{\boldsymbol{A}}_\sigma = \begin{bmatrix} \boldsymbol{A}_\sigma & \boldsymbol{O} \\ -\boldsymbol{J}_1 & \boldsymbol{I}_3 \end{bmatrix}, \ \tilde{\boldsymbol{B}}_\sigma = \begin{bmatrix} \boldsymbol{B}_\sigma \\ \boldsymbol{J}_2 \end{bmatrix}, \ \tilde{\boldsymbol{w}} = \begin{bmatrix} \boldsymbol{p}_h \\ \boldsymbol{p}_k \end{bmatrix}, \tag{8}$$

where $\tilde{\boldsymbol{A}}_\sigma \in \mathbb{R}^{(n_\sigma+3),6}$, $\tilde{\boldsymbol{B}}_\sigma \in \mathbb{R}^{(n_\sigma+3),n}$, and $\tilde{\boldsymbol{w}} \in \mathbb{R}^{6,1}$. We use (7) as the kinematic model. In the model, $\tilde{\boldsymbol{w}}$ is the regulated variable. We use both the angular velocity of the joint $\dot{\boldsymbol{\phi}}$ and the mode σ as control input. Here, the singular configurations I and II are related to the full column rankness of $\tilde{\boldsymbol{A}}_\sigma$ and the full row rankness of $\tilde{\boldsymbol{B}}_\sigma$ in equation (7), respectively. The details of these singular configurations are discussed in Section IV.A.

IV. Controller Design

The objective of the proposed controller is that the first and second control points track the respective target trajectory simultaneously. Thus, the main control objective is that $\tilde{\boldsymbol{w}}$ tracks the target trajectory $\tilde{\boldsymbol{w}}_d(t)$. Figure 3 shows a diagram of the proposed controller. First, the mode $\sigma(t)$, which represents the allocations of grounded/lifted wheels, is selected (Selecting mode in Fig. 3 and Section IV.C). The kinematic model is switched depending on the selected mode (Kinematic model block in Fig. 3 and Section III). The mode is updated every t_σ and is maintained until the next update. Second, the angular velocities of joints $\boldsymbol{u}_\sigma = \dot{\boldsymbol{\phi}}$ are calculated from the kinematic model (Joint input block in Fig. 3 and Section IV.A). In addition, the kinematic redundancies are used to realize the subtasks (Section IV.B). Next, the input constraint is applied to the calculated inputs to prevent unstable motions of the robot, which are caused by excessive input (Input constraint block in Fig. 3 and Section IV.D). The inputs are set to zero if the norm of the inputs exceeds the threshold. Finally, the actual robot is controlled by using the input after the input constraint is applied.

The fundamental framework of this switching controller has been proposed in [21]. The controller can accomplish trajectory tracking of the regulated variable as well as various subtasks, by using both the mode selection and redundant input, e.g., avoiding a movable obstacle [21], obstacle avoidance of the entire body of the robot [17], approximate path tracking of all joints [31], and changing the posture of the robot while maintaining the head position [32].

The subtasks in the study are (a) avoidance of joint limit violation, (b) avoidance of singular configuration I, and (c) avoidance of singular configuration II. We design the redundant input using the cost function related to subtasks (a)–(c). Subtasks (b) and (c) strongly depend on the mode because the two types of singular configurations depend on the allocation of grounded/lifted wheels. In contrast, subtask (a) is not directly related to the mode. Thus, we select the mode by using the cost function related to subtasks (b) and (c).

A. Joint Input

We set the joint angular velocity $\dot{\boldsymbol{\phi}}$ as the input $\boldsymbol{u}_\sigma$. From (7), we design the input as

$$\boldsymbol{u}_\sigma = \tilde{\boldsymbol{B}}_\sigma^\dagger \tilde{\boldsymbol{A}}_\sigma \left\{ \dot{\tilde{\boldsymbol{w}}}_d + \boldsymbol{K}_p \left(\tilde{\boldsymbol{w}}_d - \tilde{\boldsymbol{w}} \right) \right\} + \left(\boldsymbol{I} - \tilde{\boldsymbol{B}}_\sigma^\dagger \tilde{\boldsymbol{B}}_\sigma \right) k_v \boldsymbol{\eta}, \tag{9}$$

where $\tilde{\boldsymbol{B}}_\sigma^\dagger$ is the pseudo inverse matrix of $\tilde{\boldsymbol{B}}_\sigma$, $\boldsymbol{K}_p \in \mathbb{R}^{6,6}$ is the positive definite matrix related to the feedback gain, and $\boldsymbol{\eta} = [\partial V_u/\partial \phi_1, \cdots, \partial V_u/\partial \phi_n]^\top$, V_u is the cost function related to the subtasks, and $k_v > 0$ is a gain related to the redundancy. The second term of the right side of (9) is the redundant input, and contributes to the increase in V_u [17], [21]. If $\tilde{\boldsymbol{B}}_\sigma$ is the full row rank, the closed-loop system considering (7) and (9) is obtained as

$$\tilde{\boldsymbol{A}}_\sigma \left\{ \dot{\tilde{\boldsymbol{w}}}_d - \dot{\tilde{\boldsymbol{w}}} + \boldsymbol{K}_p \left(\tilde{\boldsymbol{w}}_d - \tilde{\boldsymbol{w}} \right) \right\} = \boldsymbol{0}. \tag{10}$$

If $\tilde{\boldsymbol{A}}_\sigma$ is the full column rank, $\tilde{\boldsymbol{w}}$ converges to $\tilde{\boldsymbol{w}}_d$ at $t \to \infty$.

In contrast, if $\tilde{\boldsymbol{B}}_\sigma$ is not the full row rank, $\tilde{\boldsymbol{B}}_\sigma \tilde{\boldsymbol{B}}_\sigma^\dagger \neq \boldsymbol{I}$. Then, the closed-loop system is obtained as

$$\tilde{\boldsymbol{B}}_\sigma \tilde{\boldsymbol{B}}_\sigma^\dagger \tilde{\boldsymbol{A}}_\sigma \left\{ \dot{\tilde{\boldsymbol{w}}}_d + \boldsymbol{K}_p \left(\tilde{\boldsymbol{w}}_d - \tilde{\boldsymbol{w}} \right) \right\} - \tilde{\boldsymbol{A}}_\sigma \dot{\tilde{\boldsymbol{w}}} = \boldsymbol{0}. \tag{11}$$

Thus, it is not ensured that the regulated variable converges to the target. Even if $\tilde{\boldsymbol{B}}_\sigma$ is the full row rank, it is not ensured that $\tilde{\boldsymbol{w}}$ converges to $\tilde{\boldsymbol{w}}_d$ when $\tilde{\boldsymbol{A}}_\sigma$ is not the full column rank in (10). Here, only the head of a snake robot is controlled in traditional studies [17], [19], [21], [29]–[32]. The kinematic model in these studies is represented by equation (4). Then, $\boldsymbol{B}_\sigma$ is always a full row rank matrix because of its elements. Thus, the singular configuration I depends only on the full rankness of $\boldsymbol{A}_\sigma$, and does not depend on $\boldsymbol{B}_\sigma$ [29]. In contrast, not only the full rankness of $\tilde{\boldsymbol{A}}_\sigma$ but also the full rankness of $\tilde{\boldsymbol{B}}_\sigma$ may be impaired in this study. From (8), the full column rankness of $\tilde{\boldsymbol{A}}_\sigma$ depends on $\boldsymbol{A}_\sigma$. It implies that the singular configuration related to the column rankness of $\tilde{\boldsymbol{A}}_\sigma$ is singular configuration I as in [29]. In contrast, the singular configuration related to the full row rankness of $\tilde{\boldsymbol{B}}_\sigma$ is singular configuration II. We have not analyzed the specific condition where the robot is in singular configuration II. However, it is experimentally verified that the robot's configuration at which $\tilde{\boldsymbol{B}}_\sigma$ is not the full row rank. For example, $\tilde{\boldsymbol{B}}_\sigma$ is not the full row rank in Figure 4 when the second control point is the center of the wheel axle on the tail. The second control point

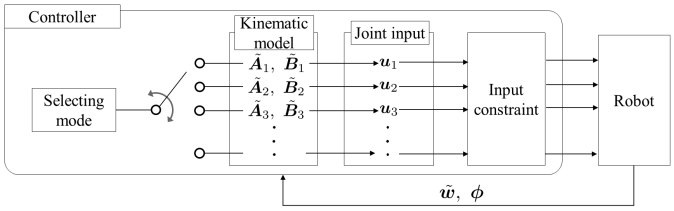

Fig. 3. Control diagram of proposed controller.

cannot move in the positive direction of the x axis without side-slipping of wheels. However, the second control point can move in the positive direction of the x axis if at least one of the first–fifth wheels is lifted. When the robot is in the neighborhood of singular configuration II, the joint input diverges because the singular value of $\tilde{\boldsymbol{B}}_\sigma$ becomes highly marginal.

B. Redundant Input

The redundant input is used to achieve the subtasks. Let $V_{u,1}$, $V_{u,2}$, and $V_{u,3}$ be the cost functions related to the prevention of joint limit violation, of singular configuration I, and of singular configuration II, respectively. We design V_u as

$$V_u = k_{u,1}V_{u,1} + k_{u,2}V_{u,2} + k_{u,3}V_{u,3}, \quad (12)$$

$$V_{u,1} = -\sum_{k=1}^{n} f\left(c_\phi, |\phi_k|\right), \quad (13)$$

$$V_{u,2} = \det\left(\tilde{\boldsymbol{A}}_\sigma^\top \tilde{\boldsymbol{A}}_\sigma\right), \quad (14)$$

$$V_{u,3} = \det\left(\tilde{\boldsymbol{B}}_\sigma \tilde{\boldsymbol{B}}_\sigma^\top\right), \quad (15)$$

$$f(x,y) = \begin{cases} (y-x)^2, & (\text{if } x < y) \\ 0, & (\text{otherwise}) \end{cases} \quad (16)$$

where $k_{u,1}$, $k_{u,2}$, $k_{u,3}$, and c_ϕ are positive weight constants. The magnitude of the joint angles can be decreased by increasing $V_{u,1}$ [32]. The singular values of $\tilde{\boldsymbol{A}}_\sigma$ increase by increasing $V_{u,2}$. Thus, it can be expected to avoid the singular configuration I by increasing $V_{u,2}$ [17], [21]. Similarly, the singular values of $\tilde{\boldsymbol{B}}_\sigma$ increase by increasing $V_{u,3}$, and it can be expected to avoid the singular configuration II by increasing $V_{u,3}$. It can be expected to achieve subtasks by increasing V_u. The robot can operate just by adjusting $k_{u,1}$, $k_{u,2}$, and $k_{u,3}$ so that the order of V_{u_1}, V_{u_2}, and V_{u_3} match. The robot may move more effectively by using the optimal weights. However, it is difficult to define the optimal weights analytically because of complexity of the cost function and the control model. The detailed analysis on optimal weights is a future work.

C. Selecting Mode

The mode is selected considering subtasks (b) and (c). Singular configurations I and II are related to the full rankness of $\tilde{\boldsymbol{A}}_\sigma$ and $\tilde{\boldsymbol{B}}_\sigma$, respectively. Thus, we select the mode using the cost function related to the singular value obtained by the singular value decomposition of these matrices. Let $\boldsymbol{s}_{\sigma,A} \in \mathbb{R}^{6,1}$ and $\boldsymbol{s}_{\sigma,B} \in \mathbb{R}^{n_\sigma+3,1}$ be the vectors composed of the singular values of $\tilde{\boldsymbol{A}}_\sigma$ and $\tilde{\boldsymbol{B}}_\sigma$, respectively. If $\boldsymbol{s}_{\sigma,A}$ and $\boldsymbol{s}_{\sigma,B}$ contain zero as the element, the robot is in a singular configuration. Therefore, we design the cost function related to selecting modes V_m as

$$V_m = k_{m,1}\min(\boldsymbol{s}_{\sigma,A}) + k_{m,2}\min(\boldsymbol{s}_{\sigma,B}), \quad (17)$$

where $k_{m,1}$ and $k_{m,2}$ are weight constants and $\min(\boldsymbol{x})$ is the function for obtaining the minimum value from the vector $\boldsymbol{x}$. By selecting the mode in which V_m in (17) is large, the mode in which the minimum singular values of the model matrices are large is selected. Thus, a mode which is far from the singular configurations is selected. Similarly to the weights for redundant input, it is difficult to decide the optimal weights for selecting mode. The robot can operate by adjusting the weight in the same way as the weights for redundant input.

Here, we consider inappropriate mode candidates. If the wheel of the second control point is grounded, the velocity constraint prevents any movement of the second control point. The full column rankness of $\tilde{\boldsymbol{A}}_\sigma$ and the full row rankness of $\tilde{\boldsymbol{B}}_\sigma$ are necessary for the avoidance of the singular configurations. Thus, the condition $n_\sigma + 3 \geq 6$ is obtained from the size of $\tilde{\boldsymbol{A}}_\sigma$, and $n_\sigma + 3 \leq n$ is obtained from the size of $\tilde{\boldsymbol{B}}_\sigma$. It is difficult to lift many adjacent pairs of wheels because of the torque limit of the actuator of the experimental robot. Therefore, the mode candidates are defined by the following conditions.

(i) The pair of wheels on the wheel axle, on which the second control point is, is lifted.
(ii) $3 \leq n_\sigma \leq n-3$,
(iii) The robot simultaneously lifts fewer than or a number equal to n_c adjacent pairs of wheels.

where n_c is a positive integer. These conditions are essential conditions for controlling the robot by using the proposed method. If these conditions are not satisfied, the convergence of the controlled variable is not guaranteed. Many modes satisfy these conditions. The computational cost becomes large because it increases depending on the number of mode candidates increases. Thus, the constraint condition (ii) is replaced as follows to reduce the computational cost.

(ii') $n_g \leq n_\sigma \leq n - n_l$,

where $n_l \geq 3$, $n_g \geq 3$ are positive integers. For example, the number of mode candidates is 66 when $n = 9$, $n_l = 4$, $n_g = 4$, and $n_c = 2$.

The mode σ is selected every t_σ seconds considering the cost function V_m. If t_σ is large, the cycle of the mode selection becomes large and may result in a delay for the robot to resume from a singular configuration. If t_σ is small, the robot can resume from the singular configuration quickly. However, frequent mode changes will require corresponding frequent control model changes. This will result in discontinuous control input changes (when the control model switches) and the control inputs become discrete. Therefore, t_σ must not be too small. The larger V_m is, the more challenging it is for the robot to be in the singular configuration. Thus, we introduce the following optimal problem in the selecting mode to select the mode where V_m is large.

$$\max_{\sigma_k} \ J, \quad (18)$$

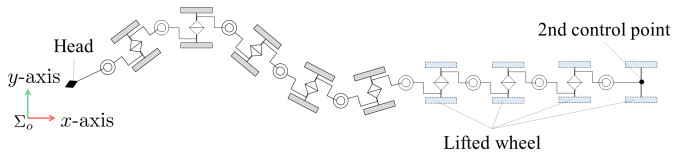

Fig. 4. An example of singular configuration II.

where

$$J = \varphi\left(\hat{\boldsymbol{q}}\left(t_p, \sigma_k\right)\right) + \int_{t_k}^{t_p} \Gamma\left(\hat{\boldsymbol{q}}\left(\tau, \sigma_k\right), \boldsymbol{u}\left(\tau, \sigma_k\right)\right) d\tau, \quad (19)$$

$\hat{\boldsymbol{q}} \in \mathbb{R}^{2n+2,1}$ is the estimated vector of $\boldsymbol{q} = \left[\boldsymbol{p}_h^\top, \boldsymbol{\phi}^\top\right]^\top$, and $t_p \geq t_k$ is a predictive horizon. The mode is selected by predicting the motion of the robot between $t_k \leq t \leq t_p$. If $t_p = t_{k+1}$, (18) is equal to the optimal problem in [30]. In the mode selection, we obtain the optimal mode $\sigma(t) = \sigma_k$ at $t = t_k$ by numerically solving (18). σ_k is maintained at $t_k \leq t < t_{k+1}$. The calculation amount increases in proportion to both the number of mode candidates and the predictive horizon t_p. In this study, we set $\varphi = \Gamma = V_m$ and $t_p = t_k$ to decrease the calculation amount.

D. Input Constraint

Even if both the redundant input and mode selection are used, it is challenging for the robot to completely prevent singular configuration. In addition, if the robot is in the neighborhood of singular configuration II, the joint input (9) becomes excessively large. Thus, we introduce the input constraint as

$$\boldsymbol{u}_\sigma = \begin{cases} \boldsymbol{0}, & (\text{if } ||\boldsymbol{u}_\sigma|| > u_{\lim}) \\ \boldsymbol{u}_\sigma. & (\text{otherwise}) \end{cases} \quad (20)$$

In the case wherein (20) is used, if the norm of the input $\boldsymbol{u}_\sigma$ exceeds a threshold $u_{\lim}$, the robot stops moving because of $\boldsymbol{u}_\sigma = \boldsymbol{0}$. Then, the robot has an opportunity to resume its motion every t_σ seconds because of the switching modes. $\tilde{\boldsymbol{A}}_\sigma$ and $\tilde{\boldsymbol{B}}_\sigma$ change when the mode is switched. If the mode wherein the robot can resume its motion exists in the mode candidates, the robot resumes its motion. In the case wherein the number of modes, it is little that the robot is in the singular configuration in the all mode candidates. Thus, it can be expected that the resume of the motion by switching mode. The norm of input is calculated using Equation (9) and depends on a variety of factors such as the target velocity of the control points, number of joints, and control gain. Therefore, it is difficult to express $u_{\lim}$ analytically. If $u_{\lim}$ is too small, the motion of the robot comes to a halt due to input constraints, even though it is not in a singular configuration. If $u_{\lim}$ is too large, the robot moves along an unintended path when the robot's posture is close to a singular configuration. Therefore, a value that is neither too high nor too low to avoid both these problems is used as $\boldsymbol{u}_{lim}$.

V. Experiments

We carried out experiments to verify the effectiveness of the proposed controller. Figure 5 shows the experimental system. The serial controlled servo motors XH430-V350-R (Dynamixel, ROBOTIS, Inc.) are used for constructing the robot. These motors are controlled by serial communication from the computer, and present angles can be obtained. The motors are serially connected by frames which are provided from ROBOTIS. The number of wheels is $n = 9$, link length is $l = 0.0685$[m], joint limit is $\phi_{\lim} = \frac{\pi}{2}$[rad]. We have designed these parameters refer to previous researches [21],

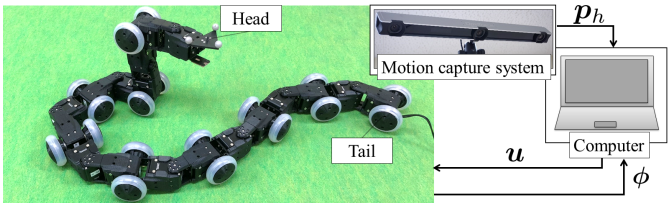

Fig. 5. Experimental system.

[22]. The marker is mounted on the robot's head, and the position and orientation of the head can be obtained by the motion capture system. The motion capture system, a pre-calibrated V120:Trio (OptiTrack, NaturalPoint, Inc.) is used in the experiments. The tracking error of the motion capture system is under 1[mm], and is sufficiently accurate for the experiments. The motion capture is updated approximately every 8 ms (120 Hz) by Motive (Optitrack, NaturalPoint, Inc.). Motive is an independent system and runs in the background on the controller. The latest captured values are used in the controller. We set sampling time of the controller as $\delta t = 0.05$[s], and end-time of the motion as $t_{\text{end}} = 120$[s]. The second control wheel is the tail wheel. Let $\tilde{\boldsymbol{w}}_0$ be the initial vector of the regulated variable; the target trajectory $\tilde{\boldsymbol{w}}_d(t)$ is designed as

$$\tilde{\boldsymbol{w}}_d(t) = \tilde{\boldsymbol{w}}_0 + \frac{\tilde{\boldsymbol{w}}_e - \tilde{\boldsymbol{w}}_0}{t_{\text{end}}} t, \quad (21)$$

where $\tilde{\boldsymbol{w}}_e \in \mathbb{R}^{6,1}$ is an arbitrary vector representing the terminal target. The position and orientation of the second control point is calculated using the position and orientation of the head and joint angles. We set $\tilde{\boldsymbol{w}}_e = \left[-0.4, -0.4, \frac{\pi}{2}, -0.8, -0.4, -\frac{\pi}{2}\right]^\top$. Let us define $c_\phi = \frac{\pi}{4}$, $t_\sigma = 2$, $n_l = 4$, $n_g = 4$, $n_c = 2$, and $u_{\lim} = 4$. Then, the number of mode candidates is 66. We set the gain as $\boldsymbol{K}_p = 4\boldsymbol{I}_6$, $k_v = 2$, $k_{u,1} = 0.6$, $k_{u,2} = 0.8$, $k_{u,3} = 0$, $k_{m,1} = 0$, $k_{m,2} = 1$. In this condition, the joint input becomes excessively large when $V_m = 0.005$, and the input constraint acts. The initial joint angles are $\boldsymbol{\phi}(0) = \left[\frac{\pi}{6}, -\frac{\pi}{6}, -\frac{\pi}{6}, 0, \frac{\pi}{6}, 0, 0, \frac{\pi}{6}, \frac{\pi}{6}\right]^\top$, and the initial position and orientation as $\boldsymbol{p}_h(0) = [0, 0, \pi]^\top$. Arbitrary initial conditions can be used, except for the special condition (e.g. singular configuration, self collision).

Figure 6 shows the experimental result. The motion of the robot in the experiments can be shown in the supplementary movie. Let e_i $(i = 1, \cdots, 6)$ be the error between the desired and actual value of ith element of the controlled variables. From Fig. 6(c), the error of all the regulated variables are small. Thus, the control points tracked the each target trajectory. The robot avoided the mode where V_m was marginal, by switching the mode. Thus, subtasks (b) (avoidance of singular configuration I) and (c) (avoidance of singular configuration II) were satisfied. All the joints did not exceed the angle limitation as in Fig. 6(d), and subtask (a) (avoidance of joint limit violation) was satisfied. As a result, it was verified that the trajectory tracking of the two control points and subtasks (a)–(c) were satisfied by the proposed controller.

From condition (ii), the number of wheels that touch the ground is $4 \leq n_\sigma \leq 5$ in the experiment. However, all the

modes selected in the experiment were $n_\sigma = 4$. It implies that the robot selects the mode wherein the number of lifted wheels is higher and that the robot has more redundant degrees-of-freedom. Although the number of candidates of the mode is 66, the number of modes selected in the experiment is 14. Therefore, it leaves a margin for improvement in the method for selecting the mode.

VI. Applications

We carried out two experiments involving the application of the controller; one is the transport of an object using the robot's body without neither the head nor tail, and the other is the steering of a handcart.

A. Caging Transport

In the experiment, the robot envelopes an object by using its entire body, such as by caging [28], and transports it by locomoting by maintaining a caging grasp. The constants and gains are equal to those in section V. We use $\boldsymbol{\phi}(0) = \left[0, \frac{\pi}{9}, \frac{\pi}{9}, \frac{\pi}{6}, \frac{\pi}{9}, \frac{\pi}{6}, \frac{\pi}{6}, \frac{\pi}{6}, 0\right]^\top$ as the initial value, and the initial position and orientation of the robot's head are equal to those in section V. The target trajectory of the regulated variable is designed as being straight ahead in the x axis direction.

Figure 7 shows the result. The error of all the regulated variables are small, and the control points tracked the each target trajectory. Therefore, it was verified that the robot could perform the caging transportation task by the proposed controller.

B. Steering a Handcart

In this experiment, we regulate the robot using the three-dimensional model derived in Appendix. The control variables are the three-dimensional positions and orientations of the head and tail of the robot in the model. The robot steers a handcart by pushing a handle using the two control points. If the robot does not maintain the relative position and orientation between the two control points, the control point separates from the pipe of the handcart, and the handcart cannot be steered. The relative position between the two points can be maintained using the proposed control method. In the case wherein the robot ' s motion is three-dimensional, the robot requires more degrees-of-freedom than in the case of two-dimensional motion. Thus, we used the robot of $n = 15$. Let $\bar{\boldsymbol{p}}_h \in \mathbb{R}^{6,1}$ and $\bar{\boldsymbol{p}}_t \in \mathbb{R}^{6,1}$ be the positions and orientations of the head and tail, respectively. The orientation is represented as the roll, pitch, and yaw. Let (R_h, P_h, Y_h) and (R_t, P_t, Y_t) be the orientation of the head and tail, respectively. The target trajectory of the regulated variable is designed as being straight ahead in the x axis direction.

Figure 8(a) shows the result of steering the handcart. The error of all the regulated variables are small, and the control points tracked the each target trajectory. Therefore, it was verified that the robot could steer the handcart by the proposed controller.

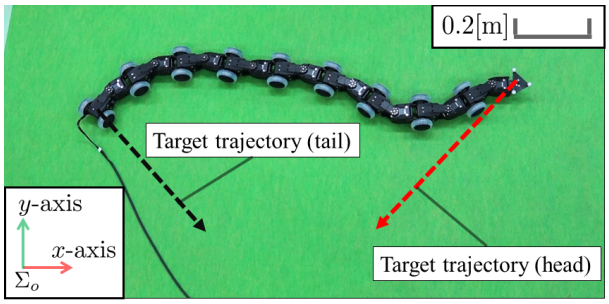

(a) The initial condition of the experiment.

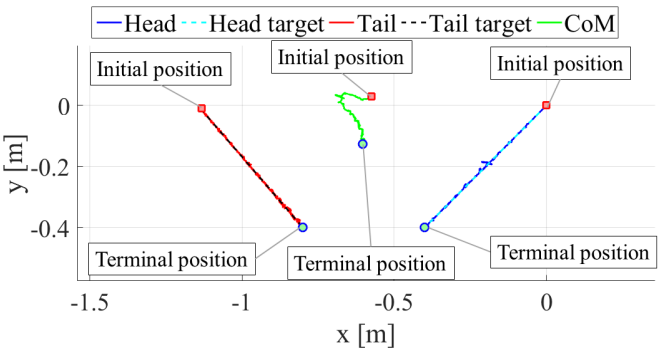

(b) Path of the control points and CoM of the robot.

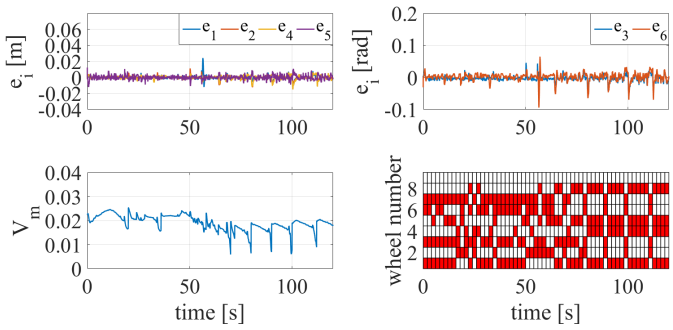

(c) Time response of the controlled variables, the cost function, the grounded/lifted state of each wheel. e_i represents the error of ith element of the controlled variables. V_m represents the evaluation value for selecting mode. The red squares represent grounded wheel.

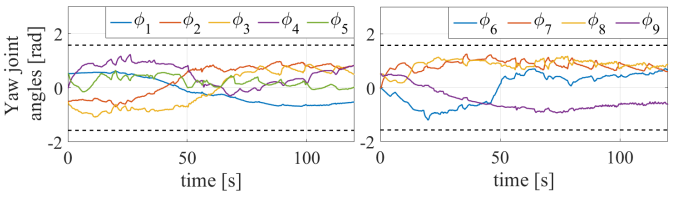

(d) Time response of the yaw joint angles. ϕ_i represents ith yaw joint angle. The dotted line represents the limit angle.

Fig. 6. Experimental results of trajectory tracking.

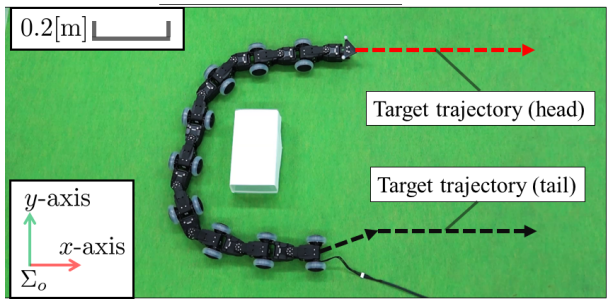

(a) The initial condition of the experiment.

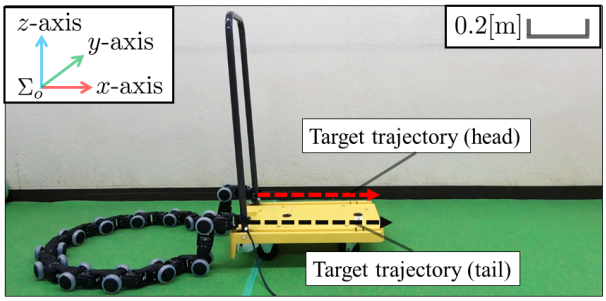

(a) The initial condition of the experiment.

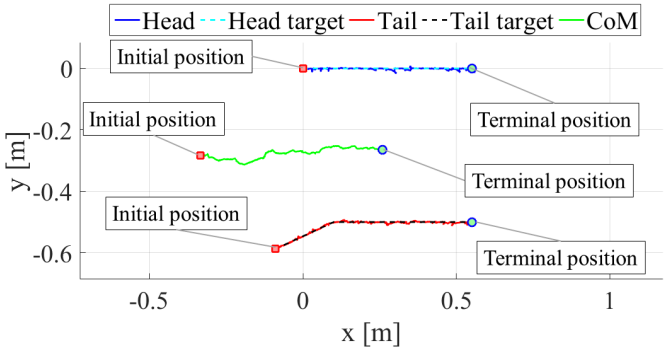

(b) Path of the control points and CoM of the robot.

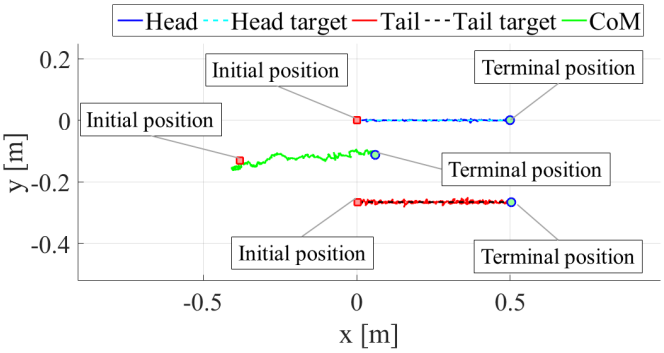

(b) Path of the control points and CoM of the robot.

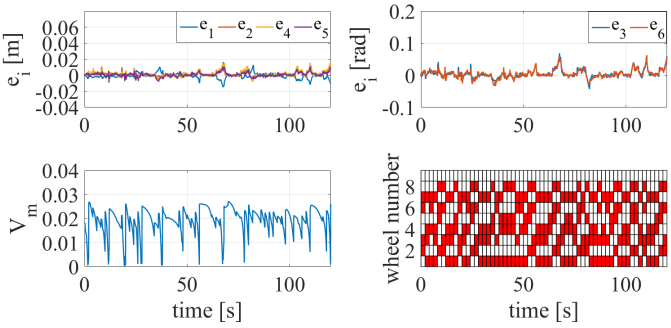

(c) Time response of the controlled variables, the cost function, the grounded/lifted state of each wheel. e_i represents the error of ith element of the controlled variables. V_m represents the evaluation value for selecting mode. The red squares represent grounded wheel.

Fig. 7. Experimental result of caging transport.

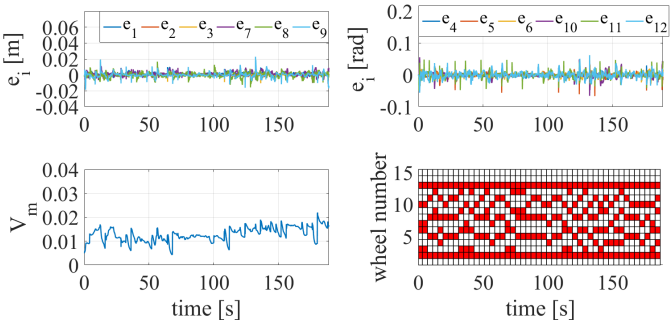

(c) Time response of the controlled variables, the cost function, the grounded/lifted state of each wheel. e_i represents the error of ith element of the controlled variables. V_m represents the evaluation value for selecting mode. The red squares represent grounded wheel.

Fig. 8. Experimental results of handcart steering.

VII. Conclusion

We presented a control method that simultaneously regulates two control points on the body of a snake robot. We derived the kinematic model, which considers the head as well as an additional point, and proposed a controller that causes the two control points to converge to the target trajectory. In this method, switching modes and redundant input were used to prevent two types of singular configurations. The experimental results demonstrated the effectiveness of the proposed method. In addition, object transport based on caging manipulation and handcart steering, which could not be realized by traditional control methods, were accomplished as applications.

Future works will improve the decision method of the mode candidates and will customize the use of both the redundant input and mode selection according to each application.

Appendix

We derive a kinematic model in which the two control points move three-dimensionally. Note that the second control point is the tail of the robot, and the other point cannot be used as the second control point.

It is necessary to introduce certain pitch joint angles into the model to regulate the three-dimensional position and orientation. We introduce the $1, 2, \cdots, n_h$th and $n_s, n_s + 1, \cdots, n-1$th pitch joint angles into the model; these pitch joints are used to lift the head and tail from the ground. Then, the $1, 2, \cdots, n_h - 1$th and $n_s, n_s + 1, \cdots, n-1$th wheels are lifted, and they do not touch the ground. Let us define the vector composed of the yaw angles and pitch angles for lifting the head and tail to be $\bar{\boldsymbol{\phi}} \in \mathbb{R}^{n_j,1}$; here, $n_j = n + n_h + n_s$.

Let $\bar{\boldsymbol{p}}_h \in \mathbb{R}^{6,1}$ be the three-dimensional position and orientation. From [22], the kinematic relationship related to the head is obtained as

$$\boldsymbol{A}_\sigma^{'} \dot{\bar{\boldsymbol{p}}}_h = \boldsymbol{B}_\sigma^{'} \dot{\bar{\boldsymbol{\phi}}}, \tag{22}$$

where $\boldsymbol{A}^{'} \in \mathbb{R}^{n_\sigma+3,6}$ and $\boldsymbol{B}^{'} \in \mathbb{R}^{n_\sigma+3,n_j}$. Let $\bar{\boldsymbol{p}}_t \in \mathbb{R}^{6,1}$ be the three-dimensional position and orientation; the kinematic relationship is obtained as

$$\dot{\bar{\boldsymbol{p}}}_t = \begin{bmatrix} \boldsymbol{J}_1^{'} & \boldsymbol{J}_2^{'} \end{bmatrix} \begin{bmatrix} \dot{\bar{\boldsymbol{p}}}_h \\ \dot{\bar{\boldsymbol{\phi}}} \end{bmatrix}, \tag{23}$$

where $\boldsymbol{J}_1^{'} \in \mathbb{R}^{6,6}$ and $\boldsymbol{J}_2^{'} \in \mathbb{R}^{6,n_j}$. Considering (22) and (23), we obtain

$$\bar{\boldsymbol{A}}_\sigma \dot{\bar{\boldsymbol{w}}} = \bar{\boldsymbol{B}}_\sigma \dot{\bar{\boldsymbol{\phi}}}, \tag{24}$$

$$\bar{\boldsymbol{A}}_\sigma = \begin{bmatrix} \boldsymbol{A}_\sigma^{'} & \boldsymbol{O} \\ -\boldsymbol{J}_1^{'} & \boldsymbol{I}_6 \end{bmatrix}, \ \bar{\boldsymbol{B}}_\sigma = \begin{bmatrix} \boldsymbol{B}_\sigma^{'} \\ \boldsymbol{J}_2^{'} \end{bmatrix}, \ \bar{\boldsymbol{w}} = \begin{bmatrix} \bar{\boldsymbol{p}}_h \\ \bar{\boldsymbol{p}}_t \end{bmatrix}, \tag{25}$$

where $\bar{\boldsymbol{A}} \in \mathbb{R}^{n_\sigma+9,12}$ and $\bar{\boldsymbol{B}} \in \mathbb{R}^{n_\sigma+9,n_j}$. We use (24) as the kinematic model for the three-dimensional motion of the two control points. The three-dimensional trajectory tracking of the two control points can be achieved by using the joint input as (9).

ACKNOWLEDGMENT

This work was partially supported by the ImPACT Program of Council for Science, Technology and Innovation (Cabinet Office, Government of Japan) and JSPS KAKENHI Grant Number 18K04011. We would like to thank Editage (www.editage.jp) for English language editing.

REFERENCES

[1] M. Travers, J. Whitman, P. Schiebel, D. Goldman, and H. Choset, "Shape-Based Compliance in Locomotion," *Proc. Robotics: Science and Systems*, 2016.

[2] T. Takemori, M. Tanaka, and F. Matsuno, "Gait Design of a Snake Robot by Connecting Curve Segments and Experimental Demonstration," *IEEE Trans. Robotics*, vol.34, issue 5, pp.1384-1391, 2018.

[3] A. Crespi and A. J. Ijspeert, "Online Optimization of Swimming and Crawling in an Amphibious Snake Robot," *IEEE Trans. Robotics*, vol.24, issue 1, pp.75-87, 2008.

[4] J. Sverdrup-Thygeson, E. Kelasidi, K. Y. Pettersen, and J. T. Gravdahl, "The Underwater Swimming Manipulator–A Bioinspired Solution for Subsea Operations," *IEEE J. Oceanic Engineering*, vol.43, issue 2, pp.402-417, 2018.

[5] D. Rollinson and H. Choset, "Pipe Network Locomotion with a Snake Robot," *J. Field Robotics*, vol.33, issue 3, pp.322-336, 2016.

[6] T. Kamegawa, T. Baba, and A. Gofuku, "V-shift control for snake robot moving the inside of a pipe with helical rolling motion," *Proc. 2011 IEEE Int. Symp. on Safety, Security and Rescue Robotics*, pp.1-6, 2011.

[7] M. Vespignani, K. Melo, M. Mutlu, and A. J. Ijspeert, "Compliant snake robot locomotion on horizontal pipes," *Proc. IEEE Int. Symp. Safety, Security Rescue Robotics*, 2015.

[8] P. Liljebäck, K. Y. Pettersen, Ø. Stavdahl, and J. T. Gravdahl, "A review on modelling, implementation, and control of snake robots," *Robotics and Autonomous Systems*, vol.60, issue 1, pp.29-40, 2012.

[9] S. Hirose, *Biologically Inspired Robots (Snake-like Locomotor and Manipulator)*. London, U.K.: Oxford Univ. Press, 1993.

[10] S. Toyoshima, M. Tanaka, and F. Matsuno, "A Study on Sinus-Lifting Motion of a Snake Robot With Sequential Optimization of a Hybrid System," *IEEE Trans. Automation Science and Engineering*, vol.11, issue 1, pp.139-144, 2014.

[11] M. Mori and S. Hirose, "Locomotion of 3D Snake-Like Robots -Shifting and Rolling Control of Active Cord Mechanism ACM-R3 -," *J. Robotics and Mechatronics*, vol.18, no.5, pp. 521-528, 2006.

[12] J. W. Burdick, J. Radford, and G. S. Chirikjian, "A 'sidewinding' locomotion gait for hyper-redundant robots," *Advanced Robotics*, vol.9, issue 3, pp.195-216, 1995.

[13] R. L. Hatton and H. Choset, "Sidewinding on Slopes," *Proc. IEEE Int. Conf. Robotics and Automation*, pp.691-696, 2010.

[14] R. Yoshizawa, T. Kano, and A. Ishiguro, "Realization of Snakes' Concertina Locomotion by Using 'TEGOTAE-Based Control', " *Proc. 5th Int. Conf. Living machines 2016*, pp.548-551, 2016.

[15] X. Wu and S. Ma, "Neurally Controlled Steering for Collision-Free Behavior of a Snake Robot," *IEEE Trans. Control Systems Technology*, vol.21, issue 6, pp.2443-2449, 2013.

[16] A. Mohammadi, E. Rezapour, M. Maggiore, and K. Y. Pettersen, "Maneuvering Control of Planar Snake Robots Using Virtual Holonomic Constraints," *IEEE Trans. Control Systems Technology*, vol.24, issue 3, pp.884-899, 2016.

[17] M. Tanaka, K. Kon, and K. Tanaka, "Range-sensor-based Semiautonomous Whole-body Collision Avoidance of a Snake Robot," *IEEE Trans. Control Systems Technology*, vol.23, issue 5, pp.1927-1934, 2015.

[18] P. Prautsch, T. Mita, and T. Iwasaki, "Analysis and control of a gait of snake robot," *Trans. IEEJ*, vol.120-D, pp.372-381, 2000.

[19] F. Matsuno and K. Mogi, "Redundancy Controllable System and Control of Snake Robot with Redundancy based on Kinematic Model", *Proc. IEEE Int. Conf. Decision and Control*, pp.4791-4796, 2000.

[20] F. Matsuno and H. Sato, "Trajectory Tracking Control of Snake Robots based on Dynamic Model," *Proc. IEEE Int. Conf. Robotics and Automation*, pp.3029-3034, 2005.

[21] M. Tanaka and F. Matsuno, "Control of Snake Robots with Switching Constraints: trajectory tracking with moving obstacle," *Advanced Robotics*, vol.28, issue 6, pp.415-429, 2014.

[22] M. Tanaka and F. Matsuno, "Modeling and Control of Head Raising Snake Robots by Using Kinematic Redundancy," *J. Intelligent and Robotic Systems*, vol.75, issue 1, pp.53-69, 2014.

[23] F. Matsuno and K. Suenaga, "Control of Redundant 3D Snake Robot Based on Kinematic Model," *Proc. IEEE Int. Conf. Robotics and Automation*, pp.2061-2066, 2003.

[24] M. Yamakita, M. Hashimoto, and T. Yamada, "Control of Locomotion and Head Configuration of 3D Snake Robot (SMA)," *Proc. IEEE Int. Conf. Robotics and Automation*, pp.2055-2060, 2003.

[25] S. Ma, Y Ohmameuda, K. Inoue, and B. Li, "Control of a 3-Dimensional Snake-like Robot," *Proc. IEEE Int. Conf. Robotics and Automation*, pp.2067-2072, 2003.

[26] M. Tanaka, and F. Matsuno, "Cooperative control of two snake robots," *Proc. IEEE/RSJ Int. Conf. Robotics and Automation*, pp. 404-405, 2006.

[27] M. Tanaka, K. Tadakuma, M. Nakajima, and M. Fujita, "Task-Space Control of Articulated Mobile Robots With a Soft Gripper for Operations," *IEEE Trans. on Robotics* , vol. 35, no. 1, pp.135-146, 2018.

[28] S. Makita and W. Wan, "A survey of robotic caging and its applications," *Advanced Robotics*, vol.31, issue 19-20, p.1071-1085, 2017.

[29] M. Tanaka and K. Tanaka, "Singularity Analysis of a Snake Robot and an Articulated Mobile Robot With Unconstrained Links," *IEEE Trans. on Control Systems Technology*, vol.24, issue 6, pp.2070-2081, 2016.

[30] M. Tanaka, M. Nakajima, and K. Tanaka, "Smooth control of an articulated mobile robot with switching constraints," *Advanced Robotics*, vol.30, issue 1, pp.29-40, 2016.

[31] M. Tanaka, K. Tanaka, and F. Matsuno, "Approximate Path-Tracking Control of Snake Robot Joints with Switching Constraints," *IEEE/ASME Trans. Mechatronics*, vol.20, issue 4, pp.1633-1641, 2015.

[32] M. Tanaka and K. Tanaka, "Shape Control of a Snake Robot with Joint Limit and Self-collision Avoidance," *IEEE Trans. Control Systems Technology*, vol.25, issue 4, pp.1441-1448, 2017.